Influence of density stratification on effluent plume dynamics*

Goran Lončar[1]
Gordana Beg Paklar[2]
Ivica Janeković[3]

[1] Water Research Department,
University of Zagreb,
Kačićeva 26, Zagreb 10000, Croatia;

e-mail: goran.loncar@grad.hr

[2] Institute for Oceanography and Fisheries,
Laboratory of Physical Oceanography,
Šetalište Ivana Meštrovića 63, Split 21000, Croatia;

email: beg@izor.hr

[3] Institute Ruđer Bošković,
Centre for Marine and Environmental Research,
Bijenička 54, Zagreb 10000, Croatia;

email: ivica@irb.hr

Abstract

In this study we modelled sea temperature (T), salinity (S) and density field dynamics using a 3D numerical model applied to Rijeka Bay (Croatia) in order to explore their effect on effluent plume dynamics in the vicinity of four submarine sewage outfalls when the bora wind (NE direction) is blowing. The vertical density stratification in the area studied is strongly related to the bora wind, which contributes significantly to the lowering of the pycnocline depth through enhanced

The complete text of the paper is available at http://www.iopan.gda.pl/oceanologia/

mixing in the vertical, giving rise to changes in the neutral buoyancy level. The features of near-field plume dynamics were calculated with the use of a separate near-field numerical model, using information on the vertical density distribution previously calculated using a 3D numerical model.

The results of the numerical simulations and statistical analysis of the wind data indicate a very low probability of complete water column homogenization and consequent effluent plume rise to the sea surface under the influence of the bora wind during the peak tourist season (May–September).

List of symbols:

A	–	characteristic area of plume cross-section
a, b	–	Ångström law coefficients
b	–	characteristic radius of plume cross-section
b_0	–	initial radius of plume cross-section at the position of diffuser nozzles
B	–	buoyancy flux
d	–	nozzle diameter
D_i	–	i-th value of a random variable
$\widehat{D}$	–	random variable of the 7.5 m s^{-1} wind speed duration
F_i	–	the cumulative absolute frequency of the i-th value of random variable $\widehat{D}$
k	–	turbulent kinetic energy (TKE)
M	–	specific momentum flux
n	–	the number of samples
$P(\widehat{D} \geq D_i)$	–	probability of reaching or exceeding the value D_i of a random variable $\widehat{D}$,
S	–	sea salinity
T	–	sea temperature
T	–	specific buoyant force per unit plume length
u	–	velocity in the centre of the plume cross-section
ε	–	turbulent kinetic energy dissipation
θ	–	angle of inclination of a tangent of a plume trajectory to the horizontal axis
θ_0	–	angle between nozzle symmetry axes and horizontal plane
λ	–	dispersion ratio of transport scalar quantities
ρ	–	density along the central trajectory of a plume
ρ_m	–	sea density
ρ_{m0}	–	sea density at the position of diffuser nozzles
$\Delta\rho$	–	density deficit
σ_t	–	density anomaly
ϕ	–	volume flux
ψ	–	mass flux

1. Introduction

Effluent transport phenomena in the aquatic environment are interdisciplinary problems (Fischer et al. 1979). Traditional fluid mechanics focuses on project solution optimization and analyses of structural operability. On the other hand, geophysical fluid mechanics (meteorology, oceanography) is oriented more towards the comprehension and prediction of the relevant processes at broader temporal and spatial scales. Environmental fluid mechanics targets its major concern somewhere between these two extremes with the aim of assessing the potential environmental hazard impact and helping in decision-making processes for proposed project solutions (Cushman-Roisin et al. 2008).

Dominant forcing and its intensities in the mixing processes affecting the effluent plume on its path from the diffuser orifice to the arbitrary downstream profile are highly variable. Therefore, the concept of separating the far-field and near-field zones with different dominant forcing is widely adopted (Fischer et al. 1979). In the case of a submarine public sewage outfall, the near-field domain in the vicinity of the outfall diffuser ranges from the inflow point up to the sea surface or the neutral buoyancy layer, where further effluent plume rise is interrupted, after which plume dynamics is mainly in the horizontal direction (Akar & Jirka 1994a,b). Therefore, the integral solution of the problem is usually obtained through the combination of two structurally different numerical models. Plume propagation in the far field is modelled with a 2D or 3D oceanographic numerical model using initial concentration fields calculated from the near-field model (Wood et al. 1993, Akar & Jirka 1994a,b, Pun & Davidson 1999). Using this approach one can avoid a high-resolution numerical grid within the far-field model required for resolving the near-field mixing process. In this study we have slightly modified the previously described methodology in order to assess the influence of bora-induced density changes on effluent plume dynamics. This approach consists of two steps: a) temporal changes in the vertical density distribution along the water column at the positions of the analysed submarine outfall diffusers are obtained from 3D numerical model simulations; b) mixing processes in the near-field are resolved using a numerical model constructed according to Featherstone (1984), with previously calculated vertical density profiles. More details on the near-field numerical model used are given in section 3.

In the Rijeka Bay area (Figure 1) tourist activities and the bathing season are at their height in the summer, at the end of June and during the first half of July. Many projects and construction activities related to the implementation of municipal sewage systems as well their improvements are currently in progress. Three new submarine outfalls

L, O, MNJ (Figure 1) are envisaged for construction, and plans are in hand to extend the one already in existence R (Figure 1). The basic hydraulic characteristics of these four outfalls are given in Table 1 (Andročec et al. 2009). The hydraulics of the diffusers were taken into account according to the methodology of Fischer et al. (1979) and more recently by Bleninger (2007). It is planned that the new three outfalls L, O and MNJ will be constructed with a single pipe multinozzle diffuser and an alternating nozzle arrangement (Andročec et al. 2009). The same holds for the planned extension of the existing submarine outfall R.

Stable stratification with sea water density increasing towards the bottom prevails in summer under stable marine and atmosphere conditions
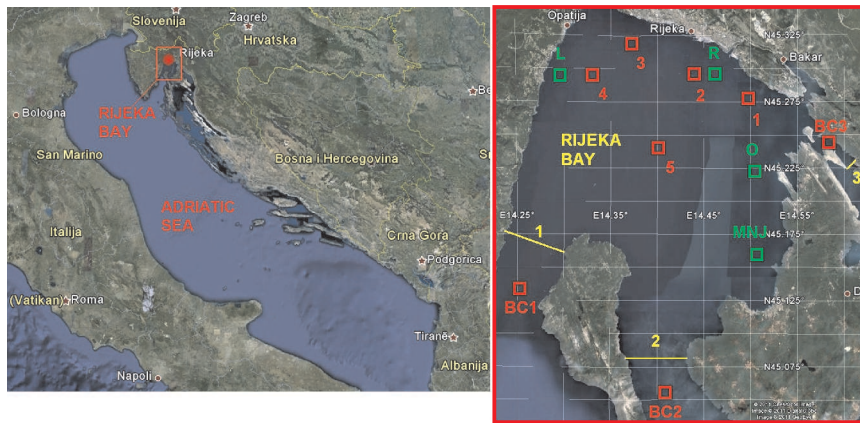

Figure 1. The domain analysed, showing the positions of the submarine outfalls L, O, MNJ, R (green rectangles), the CTD station sites 1, 2, 3, 4, 5, BC1, BC2 and BC3 measured during the monitoring programmes from 1976 and 2003–2007 (red rectangles), and the open boundary transects (yellow lines)

Table 1. Basic hydraulic characteristics of the four submarine outfalls L, O, MNJ and R according to the relevant project documentation (Andročec et al. 2009). $L_{outfall}$ is the submarine outfall length, Δl the distance between two adjacent diffuser nozzles, d the nozzle diameter, Q_{max} the maximum hourly discharge through the submarine outfall, and $L_{diffuser}$ the diffuser length

Sewage system	$L_{outfall}$ [m]	Δl [m]	d [m]	$L_{diffuser}$ [m]	Q_{max} [m^3 s^{-1}]	
					existing	planned
Rijeka (R)	500	8	0.1	250	0.6	1.0
Lovran (L)	500	10	0.1	150	0	0.31
Omišalj (O)	500	10	0.075	100	0	0.1
Malinska-Njivice (MNJ)	500	10	0.1	120	0	0.24

(Artegiani et al. 1997, Supić & Vilibić 2006), which is favourable in the sense that the effluent plume is locked in the subsurface layer. Disruption or partial cessation of the stable stratification in the area analysed may be triggered by intense wind forcing, mostly from the SE (sirocco) and the NE (bora) (Penzar & Makjanić 1978, Penzar et al. 2001).

The bora brings about a rapid drop in air temperature and humidity, and consequently an increased latent and sensible heat flux from the sea to the atmosphere, followed by a decrease in sea water temperature and a slight increase in salinity. Furthermore, strong wind-induced currents transport relatively warm surface water out of Rijeka Bay, simultaneously inducing a relatively cold subsurface inflow. During a bora event the air is extremely clear and the light intensity high (Penzar et al. 2001), which has a positive effect on the rate of bacterial decay. In view of the prevalent direction, intensity and associated fetch of the bora, wind-generated surface waves at the locations of the submarine outfalls under scrutiny here are incipient, having just a minimal effect on vertical density distribution. On the other hand, the sirocco, blowing continuously from the SE, has longer fetches, resulting in waves with greater periods, lengths and heights than those produced by the bora. Wave-induced particle movements are then possible even at the depth of the pycnocline, eroding the density gradient along it (Hydroexpert 1993). Intense sirocco winds in summer are correlated with a high air humidity, poor air transparency and reduced light intensity. Obviously, these conditions increase the probability of stratification erosion and prolong the time of bacterial decay.

Although both winds may erode the stable summer stratification, the bora, because of intense surface cooling, evaporation and mixing, is a more probable mechanism for vertical mixing in the water column and possible effluent plume rise. In this study, therefore, we decided to analyse the effect of the bora on the vertical density profile. Moreover, studies of the temporal structures before and after wind events in the northern Adriatic indicated significant changes induced by the bora, whereas no influence on the sea temperature was observed when the sirocco was blowing (Beg Paklar 2000).

The numerical modelling setup is presented in the next section, and the methodology and data used in the numerical validation are discussed in the third section. The validation of the methodology along with the remaining numerical modelling results and probability analyses are given in section 4, while the concluding remarks are given in section 5, followed by the Conclusion.

2. Numerical model setup

Numerical model solutions for the domain (shown in Figures 1 and 2) were computed using the Mike 3fm numerical model (www.dhigroup.com). This is based on a flexible mesh approach, and its hydrodynamic module solves the 3D RANS equations using the Boussinesq and hydrostatic approximations. The model uses a free surface, and vertical model discretization is carried out using the standard sigma coordinate approach (Song & Haidvogel 1994). Governing equations are solved within a finite volume frame, based on a single cell division and continuum discretization with non-overlapping elements (Sleigh & Gaskel 1998). An unstructured mesh is used in the horizontal but a sigma-structured one in the vertical. An approximate Riemann solver (Roe 1981, Toro 1997) is used to calculate convective terms, enabling computation in cases of discontinuous solutions with steep gradients. For time integration, the model uses a semi-implicit approach – explicitly in the horizontal and implicitly in the vertical. The Smagorinsky scheme (1993) and k–ε models (Rodi 1987) are used for turbulence closure formulation in the horizontal and vertical directions, respectively.

Simulations with the Mike 3fm model were run using the following parameter values: minimum time step of external mode $\Delta t = 0.1$ s, maximum time step of internal mode $\Delta t = 60$ s with a critical threshold CFL of 0.8. Dispersion coefficients (Prandtl's number) for the scalar T, S fields were defined with proportionality factor 0.09 in the vertical and 0.85 in the horizontal with respect to the scaled eddy viscosity. The proportionality factors for the dispersion coefficients of turbulent kinetic energy TKE and dissipation ε were used with the values 1 for the TKE and 1.3 for ε in the horizontal and vertical directions. Roughness and Smagorinsky coefficients were set as spatially and temporally constant values of 0.01 and 0.2, respectively. The value of 0.00123 (Wu 1994) was used for the wind friction coefficient. The relations for global radiation and insolation were defined according to Ångström's law. The correlation coefficients a and b in the Ångström law were defined according to the global mean radiation per decade for the city of Rijeka in the period 1981–2000: in this case, the constants for July were $a = 0.21$ and $b = 0.55$. A wind constant of 0.5 and an evaporation coefficient of 0.9 were used in Dalton's law. The heat flux absorption profile in the short-wave radiation is described by a modified version of Beer's law. The values used were 0.3 for the energy absorption coefficient in the surface layer and 0.092 for the light decay coefficient in the vertical direction. Surface river inflows and bottom freshwater sources were not included in the model simulations.

Figure 2 shows the finite element model grid used in the Mike 3fm model simulations. Variable grid spacing between numerical nodes ranging from 150 m to 750 m were used in the horizontal, and 20 sigma layers were used in the vertical. The importance of a high spatial resolution in the Mike 3fm model is not so pronounced, since this model is used only to analyse the dynamics of T, S, σ_t and their vertical distribution, not for modelling effluent spreading in the near or far field. Therefore, the results of Mike 3fm simulations, for the domain shown in Figure 2, were used only as 'input' for the near-field model.

The near-field effluent transport model is defined using set of differential equations for motion on steady control volume (Featherstone 1984). The core of the model assumes an initial effluent inflow through a circular nozzle and a single buoyant jet or plume propagation not interacting with any other buoyant jets or plumes from adjacent nozzles.

Volume flux ϕ, mass flux ψ, specific momentum flux M, buoyancy flux B and specific buoyant force per unit length of a plume T are expressed by integral equations (1a)–(1e), where A represents the cross-sectional area of a plume orthogonal to the central trajectory, u is the velocity in the plume cross-section, ρ the density in the plume cross-section, $\Delta\rho$ the density deficit ($\Delta\rho = \rho_m - \rho$), ρ_m the sea water density and ρ_{m0} the sea water density at the positions of the diffuser nozzles.
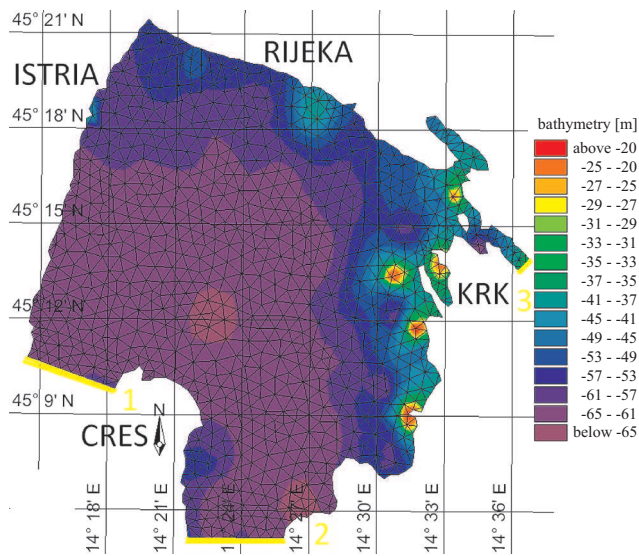

Figure 2. Finite element model grid using Mike 3fm simulations with corresponding bathymetry. The yellow lines show the model's open boundary transects

$$\phi = \int_A u \, dA, \qquad \psi = \int_A \rho u \, dA, \qquad M = \int_A u^2 \, dA, \qquad \text{(1a,b,c)}$$

$$B = g \int_A \left(\frac{\Delta \rho}{\rho_{m0}} \right) u \, dA, \qquad \text{T} = g \int_A \left(\frac{\Delta \rho}{\rho_{m0}} \right) dA. \qquad \text{(1d,e)}$$

The core of the model is contained in the definition of the rate of change for fields ϕ, ψ, M and B along the central trajectory path s of the stationary plume. Neglecting the influence of the ambient current on the overall plume dynamic, the specific momentum rate of change becomes zero in the horizontal direction (eq. (2a)). The change in the specific momentum in the vertical direction is caused by buoyancy (eq. (2b)). As a result of ambient fluid entrainment through the outer contour of the plume, volume flux and mass flux change along path s are defined by equation (3) (Turner 1986). Henceforth, the specific momentum and volume flux follow:

$$\frac{d}{ds}(M \cos \theta) = 0, \qquad \frac{d}{ds}(M \sin \theta) = \text{T}, \qquad \text{(2a,b)}$$

$$\frac{d\phi}{ds} = E = 2\pi b \, \alpha u(s), \qquad \text{(3)}$$

where $u(s) = u(s, r = 0)$ is the velocity along the central trajectory of the plume, b is the radial distance from the central trajectory to the position where the velocity takes the value of $u(s, r = b) = u(s, r = 0)/e$, $\alpha = 0.083$ is the entrainment constant (Featherstone 1984), and θ is the angle of inclination of the tangent of the plume trajectory to the horizontal axis.

One assumes a Gaussian distribution of the velocity $u(s, r)$ and density deficit $\Delta \rho(s, r)$ in the plume cross-section, where the constant $\lambda = 1.16$ in the case of scalar transport.

$$u(s, r) = u(s) e^{-r^2/b^2}, \qquad \Delta \rho(s, r) = \Delta \rho(s) e^{-r^2/(\lambda b^2)}. \qquad \text{(4a,b)}$$

Integration of equation (1) (eq. (5)) and definition of the proportionality between dB/ds and ϕ (eq. (6)) along the streamline results in:

$$\phi = \pi u(s) b^2(s), \qquad M = \frac{\pi u^2(s) b^2(s)}{2}, \qquad \text{(5a,b)}$$

$$B = \frac{\pi g \lambda^2 \Delta \rho(s) u(s) b^2(s)}{\rho_{m0}(1 + \lambda^2)}, \qquad \text{T} = \frac{\pi g \lambda^2 \Delta \rho(s) b^2(s)}{\rho_{m0}}, \qquad \text{(5c,d)}$$

$$\frac{dB}{ds} = \frac{g}{\rho_{m0}} \frac{d\rho_m}{ds} \phi. \qquad \text{(6)}$$

Substituting ϕ, M, B (eq. (5)) in equations (2), (3), (6), and using some algebraic manipulation, one obtains the system of equations (7)–(11). The abbreviated symbols u and $\Delta\rho$ are used instead of $u(s)$ and $\Delta\rho(s)$ for the sake of simplicity:

$$\frac{du}{ds} = \frac{2g\lambda^2\Delta\rho}{\rho_{m0}u}\sin\theta - \frac{2\alpha u}{b}, \tag{7}$$

$$\frac{db}{ds} = 2\alpha - \frac{g\lambda^2\Delta\rho b}{\rho_{m0}u^2}\sin\theta, \tag{8}$$

$$\frac{d\theta}{ds} = \frac{2g\lambda^2\Delta\rho}{\rho_{m0}u^2}\cos\theta, \tag{9}$$

$$\frac{d\Delta\rho}{ds} = \frac{(1+\lambda^2)}{\lambda^2}\frac{d\rho_m}{dz}\sin\theta - \frac{2\alpha\Delta\rho}{b}, \tag{10}$$

$$\frac{dx}{ds} = \cos\theta, \qquad \frac{dz}{ds} = \sin\theta. \tag{11a,b}$$

The dilution S is defined according to Fan et al. (1966):

$$S(s) = \frac{4\lambda^2 u b^2}{(1+\lambda^2)u_0 d^2}. \tag{12}$$

Integration of equations (7)–(11) begins where the Gaussian profiles (eq. (4)) are fully developed, e.g. at a distance of $s_0 = 6.2d$ (Featherstone 1984). The initial velocity $u(s = s_0 = 6.2d)$ is equal to the mean exit velocity at the diffuser nozzle $4\phi_0/(\pi d^2)$, whereas the initial plume radius is obtained from the conservation of momentum $b_0 = d/\sqrt{2}$.

The initial deflection of the nozzle axis from the horizontal plane θ_0 retains the same value up to the distance s_0 or $\theta(s = s_0 = 6.2d) = \theta_0$. The value $\theta_0 = 0^0$ is used for the numerical simulations, representing a horizontal nozzle set-up. The initial density difference at s_0 is assumed with the equality $\Delta\rho(s = s_0 = 6.2d) = \Delta\rho_0 = [(\rho_{0m} - \rho_0)(1 + \lambda^2)/(2\lambda^2)]$, the initial coordinates of the central plume trajectory with $x(s = s_0 = 6.2d) = x_0 = s_0\cos\theta_0$ or $z(s = s_0 = 6.2d) = z_0 = s_0\sin\theta_0$, and the initial dilution with $S(s = s_0 = 6.2d) = S_0 = 2\lambda^2/(1 + \lambda^2)$.

To solve the system of equations and in order to minimize local errors in the near-field model, the fourth-order Runge-Kutta method with a variable spatial step was used. The model stops the integration when the effluent plume reaches the recipient surface or exceeds the neutral buoyancy level.

It should be stressed that some commercially available modelling systems, such as Cormix V6.0 (www.mixzon.com), address the full range

of discharge geometries (single or multiport 3D orientation etc.) with different flow configurations (trapped, buoyant or sinking plumes). On the other hand, Cormix requires an analytical scheme of the vertical density distribution. The measured profile should therefore be approximated by one of three proposed stratification profile types. The performance of the near-field model described above (Featherstone 1984) is not restricted in that way, and direct use of the measured density profile is also possible.

The dilution at the end of the near field was previously calculated using the Cormix model and Featherstone's (1984) model for 20 submarine outfalls in the eastern Adriatic (Lončar 2010). In comparison with the Cormix model, the results are on average 5% (10%) greater for dilution during the summer (winter) period than in the model described and used in this study. The greater dilution obtained with the Cormix model is probably the consequence of taking ambient currents into account. Furthermore, the minor difference reported for the summer period is the result of a limited increase in buoyancy during summer stratified conditions and thus a shorter exposure to ambient currents (Lončar 2010).

3. Numerical experiments and data used

The first available data for vertical T, S and σ_t were measured at standard oceanographic depths (0, 5, 10, 20, 30, 50 m and bottom) in September 1976. The huge importance of those data is in their time of sampling: the measurements were made immediately before (03.09.1976) and after (05/06.09.1976) strong wind events from the SE and NE. Furthermore, wind speed and direction, cloudiness, air humidity and temperature were also measured at station 5 (Figure 3) with a 3-hour temporal resolution. The T and S values measured (03.09.1976 and 07.09.1976) at the CTD sites at these depths situated in the vicinity of the open boundaries BC1, BC2 and BC3 were used directly for the boundary forcing of the 3D Mike 3fm model. The time variability in T and S at the open boundary fields during the simulated period were linearly interpolated from measurements. The sea level dynamics at the open boundaries were synthesized using 7 major tidal constituents M2, S2, K2, N2, K1, O1 and P1 (Janeković et al. 2003, 2005). Unfortunately, temperature measurements were carried out at stations 1–4 only on 05.09.1976 and at station 5 only on 06.09.1976. Therefore, the initial T, S fields for the 3D model were calculated using bilinear interpolation of the T, S values measured at stations BC1, BC2 and BC3 on 03.09.1976, whereas the temperatures measured at stations 1–5 were used for the verification of the model results.

Another data set was available from the monitoring programmes conducted in the period 2003–2007. Vertical profiles of T, S and σ_t were
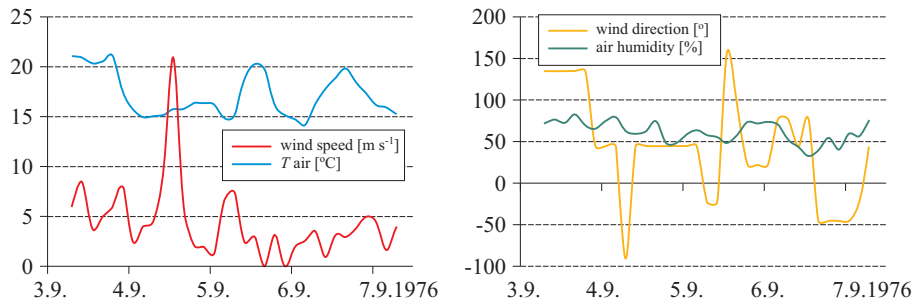
Figure 3. Air temperature and humidity, wind speed and direction measured with a three-hour temporal resolution at station 5 during the period 03.09.1976–07.09.1976

recorded with CTD probes in the central part of Rijeka Bay (station 5, Figure 1). Measurements were carried out in March, May, June, July and September (Figure 4). The primary interest in the study was related to the period from June to July because this is the height of the tourist season. The gentlest vertical density gradients were measured on 17.07.2003 with the pycnocline recorded at 5 m depth. Such a vertical density distribution is more susceptible to vertical mixing due to atmospheric forcing than the vertical profiles registered in all the other years of monitoring. Therefore, in the second step of our study, the initial and open boundary T, S 3D fields were defined on the basis of the T, S profiles measured at station 5 on 17.07.2003 (Figure 4). The T and S fields were unified in the horizontal direction across the whole model domain. At the onset of the bora wind, sea currents were flowing out mostly through open boundaries 1 and 2; hence, temporal changes of T and S in the surface layer were hard to determine. Simultaneously, a compensatory inflow through the middle and bottom layers at open boundaries 1 and 2 took place. The numerical simulations covered a period of only 48 h, so the distributions of T and S in the middle and bottom layers were subject to only a minor temporal variation through the communication with the open sea. We therefore think it is appropriate to use fixed T, S boundary conditions at open boundaries 1 and 2.

Anemometer recording of wind speed and direction at the Rijeka meteorological station ($\varphi = 45°20'$, $\lambda = 14°27'$) has been carried out continuously since 1979 and is representative of the whole domain studied. From the total data set only the wind speed and direction for the period 20 June to 20 July were analysed in detail, since the numerical analyses focused on the state of the sea in the second half of June and first half of July. The next step in filtering the data set is the criterion of the 6 h minimum duration of continuous wind with minimum hourly averaged speeds of 6.5 m s^{-1}.
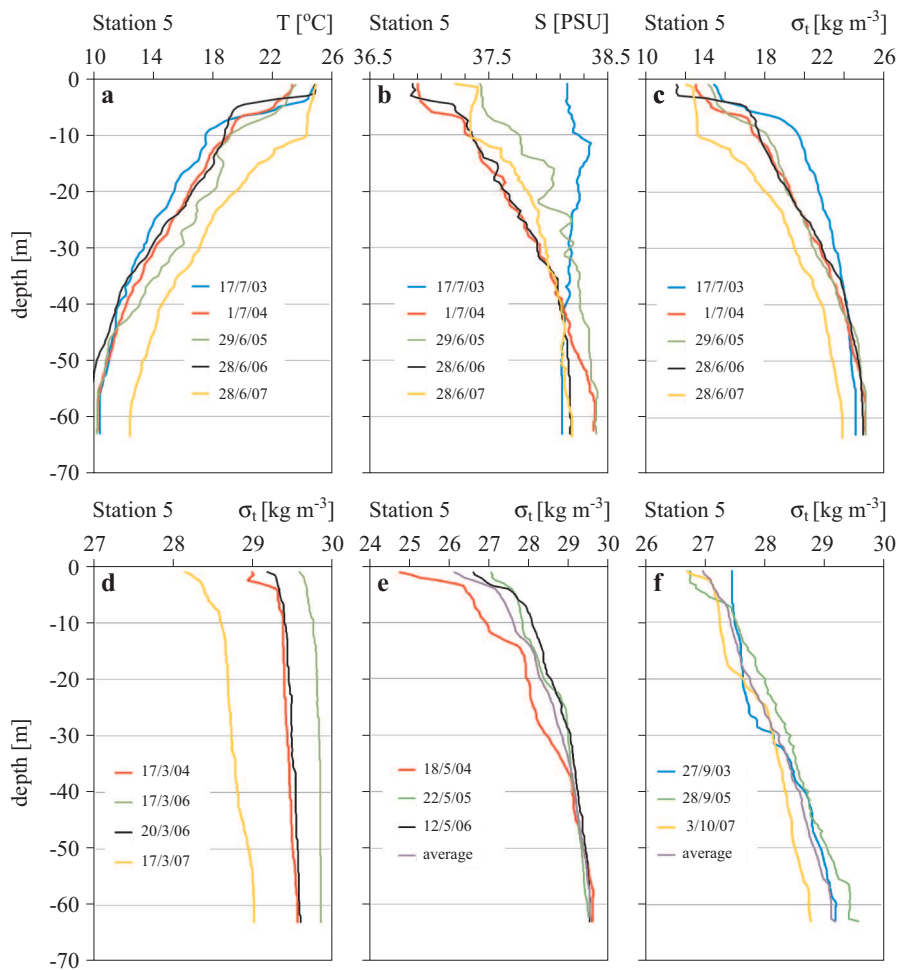
Figure 4. Vertical profiles of temperature (a), salinity (b) and density (c, d, e, f) in the central part of Rijeka Bay (station 5, Figure 1) measured in the period 2003–2007

Accordingly, all the bora wind episodes from the period 20 June to 20 July in the years 1979–2008 meeting the described criteria set formed a pattern for the prediction of extremes. It is interesting that in all the selected cases, almost all the hourly averaged wind speeds lie in a relatively narrow range of values (6.5–7.7 m s^{-1}) with a mean of 7.06 m s^{-1} and standard deviation of 0.47 m s^{-1}. Therefore, the long-term prediction was made only for the random variable 'duration of the wind – D' with a speed of 7.5 m s^{-1}. Accordingly, the results of the forecasting procedure give extreme durations with appropriate return periods, marked T_{RP}.

The long-term empirical probability distribution was calculated using the Hazen compromise formula:

$$P(\widehat{D} \geq D_i) = \frac{(2F_i - 1)}{2n}, \tag{13}$$

where $P(\widehat{D} \geq D_i)$ is the probability of reaching or exceeding the value D_i of a random variable $\widehat{D}$, $\widehat{D}$ is a random variable of the 7.5 m s^{-1} wind speed duration, D_i is the i-th value of a random variable, F_i is the cumulative absolute frequency of the i-th value of random variable $\widehat{D}$, and n is the number of samples.

After obtaining a long-term empirical log-normal probability distribution, which is well adjusted by a first-order polynomial, adaptation of the theoretical log-normal probability distribution was performed. By extrapolating the theoretical log-normal probability distribution in the area of small probabilities (large return periods), a long-term forecast for the period 20 June–20 July was made. Thus, the 48-hour duration of wind with speed 7.5 m s^{-1} corresponds to a return period of 100 years.

Apart from the June/July period analysed, T, S and σ_t dynamics were also computed for the second half of May, when the tourist season starts, and for the end of September, when it ends. The methodology of computing the initial and boundary conditions in the 3D numerical model setup is identical to that previously mentioned for the June/July period. Initial and boundary conditions for temperature and salinity are defined according the measured and averaged T, S profiles for all the years of available data (Figure 4).

Additional numerical experiments with a wind speed of 10 m s^{-1} and 48 h duration were carried out for verification purposes. It should be noted that such wind conditions are of a purely hypothetical character, as the probability of their occurrence is extremely low. Momentum, heat and water air-sea fluxes in the last four experiments were calculated assuming that the atmospheric fields – wind, air temperature, relative humidity and cloudiness – are stationary and horizontally homogeneous (Table 2). The atmospheric

Table 2. Values of the steady state atmospheric parameters used in the model simulations

	Period		
	June/July	May	Sept.
wind speed [m s^{-1}] 10 m above surface	7.5;10	7.5;10	7.5;10
air temperature [°C] 2 m above surface	21	15	15
rel. humidity [%] 2 m above surface	55	55	55
sky clearness [%]	90	90	90

parameters used in the flux calculations were determined according to the Climate Atlas of Croatia (Zaninović et al. 2008).

Sea density profiles were extracted from the 3D numerical model results at the positions of the submarine outfalls analysed with a 12 h time increment (Figure 1). These vertical profiles were used in the implemented near-field numerical model for calculating effluent mixing in the vicinity of the submarine outfalls. The near-field model supplies relevant data on the maximum vertical positions of the effluent plume above the sea bottom for successive density vertical distributions using a 12 h increment over a period of 48 h.

Since the density profiles obtained from the measurements in March were vertically well mixed, the effluent plume could reach the sea surface even without wind assistance; numerical analysis of the mixing process in the near-field was not carried out for March.

4. Results and discussion

Verification of the 3D numerical model results for the period from 3 to 7 September 1976 was carried out using the initial and boundary conditions explained in section 2. Figure 5 shows snapshots of the current velocity fields at 1, 5, 10, 20 and 30 m depth at the time coinciding with the registered wind speed maxima (21 m s^{-1} – Figure 2) from the NE. Downwind currents are found in the upper layer extending down to 20 m depth, while compensating north-eastward and eastward flows are from 20 m depth to the bottom. Figure 6 shows a comparison of the measured and modelled T profiles at oceanographic stations 1–5 (Figure 1). The differences in the middle and bottom layers at measurement site 4 are small and most likely caused by the presence of the local bottom freshwater springs typical of the area but not included in the model simulation. At station 5 the differences are the most pronounced but still small, probably due to errors in the initial vertical T profile used in the vicinity of station 5. Figures 7 and 8 show the hourly averaged current velocity fields at 1, 10 and 40 m depth during the constant wind forcing from the NE with speeds of 7.5 and 10 m s^{-1}, 24 and 48 h after the wind forcing onset. The former results refer to the period from late June until early July. The current field structure with outgoing flow in the surface layer and compensating currents below are similar in all the experiments. The main differences in the current fields are found along transect at open boundary 1 and 10 m depth (Figures 7b, 7e and 8b, 8e), where more pronounced horizontal compensation takes place in the case of wind forcing with a speed of 7.5 m s^{-1} than of 10 m s^{-1}, owing to the greater depth of the Ekman layer in the case of the stronger wind.
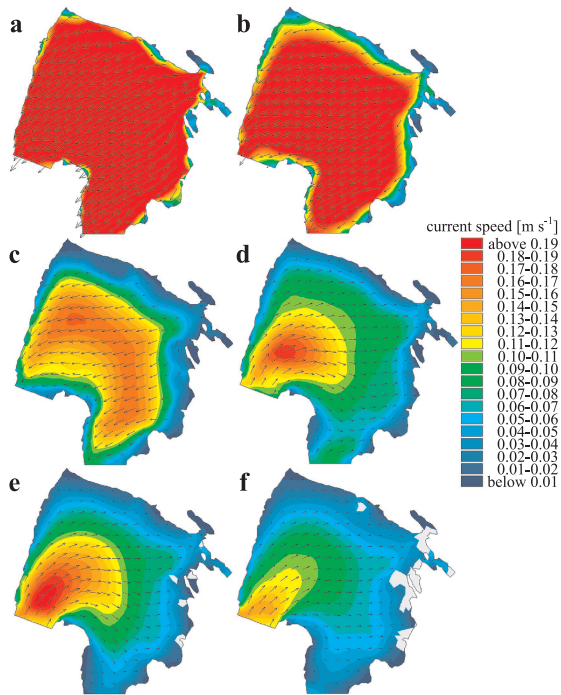
Figure 5. Snapshot of the current fields at depths of 1 m (a), 5 m (b), 10 m (c), 20 m (d), 30 m (e) and 40 m (f) at the time of the recorded NE wind speed maximum of 21 m s^{-1} on 4.09.1976 at meteorological station 5
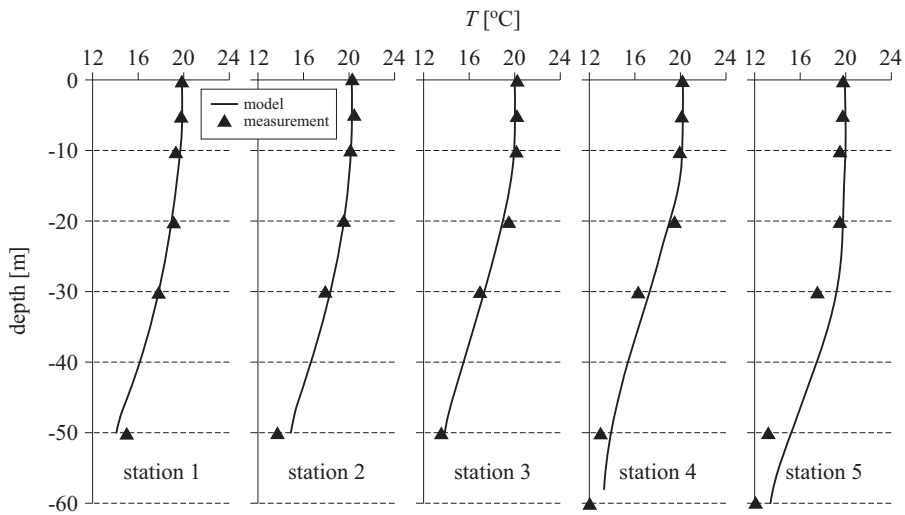

Figure 6. Comparison of measured and modelled vertical temperature profiles at oceanographic stations 1–5
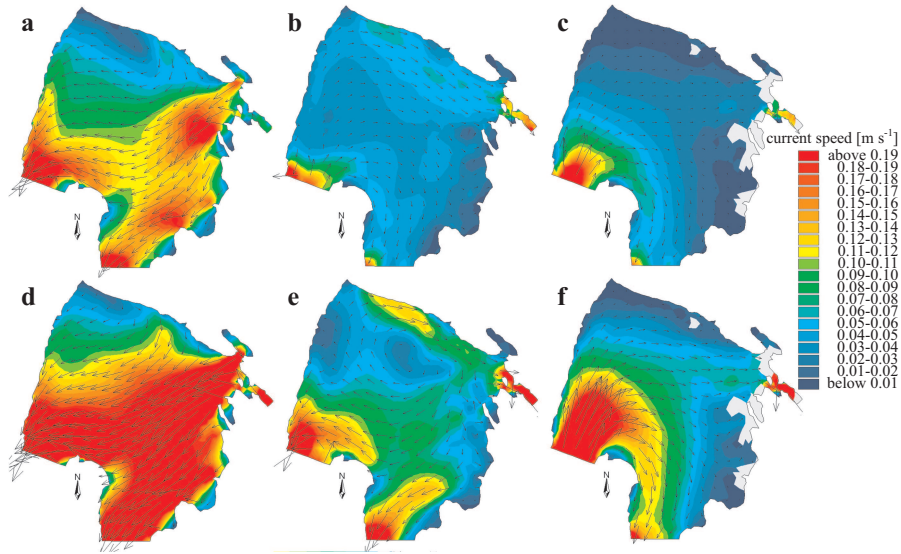
Figure 7. Hourly averaged current fields at depths of 1 m (left), 10 m (middle) and 40 m (right) during the steady wind forcing with wind speed of 7.5 m s^{-1} (above) and 10 m s^{-1} (below) 24 h after the wind onset in June/July (the colour palette used is the same as in Figure 5)
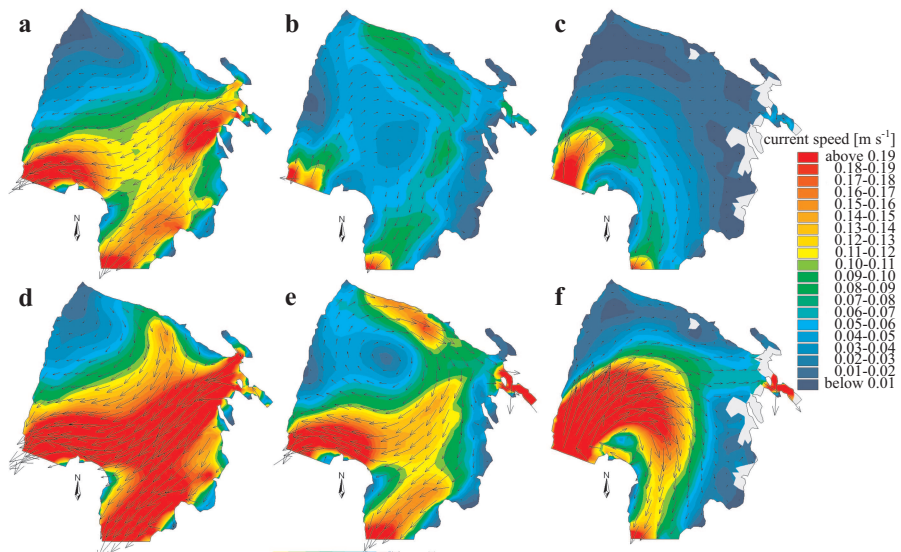

Figure 8. As for Figure 7, but for 48 hours after the wind onset

Figure 9 shows vertical density profiles at the planned locations of the submarine outfall diffusers L, R, O and MNJ during the simulation period
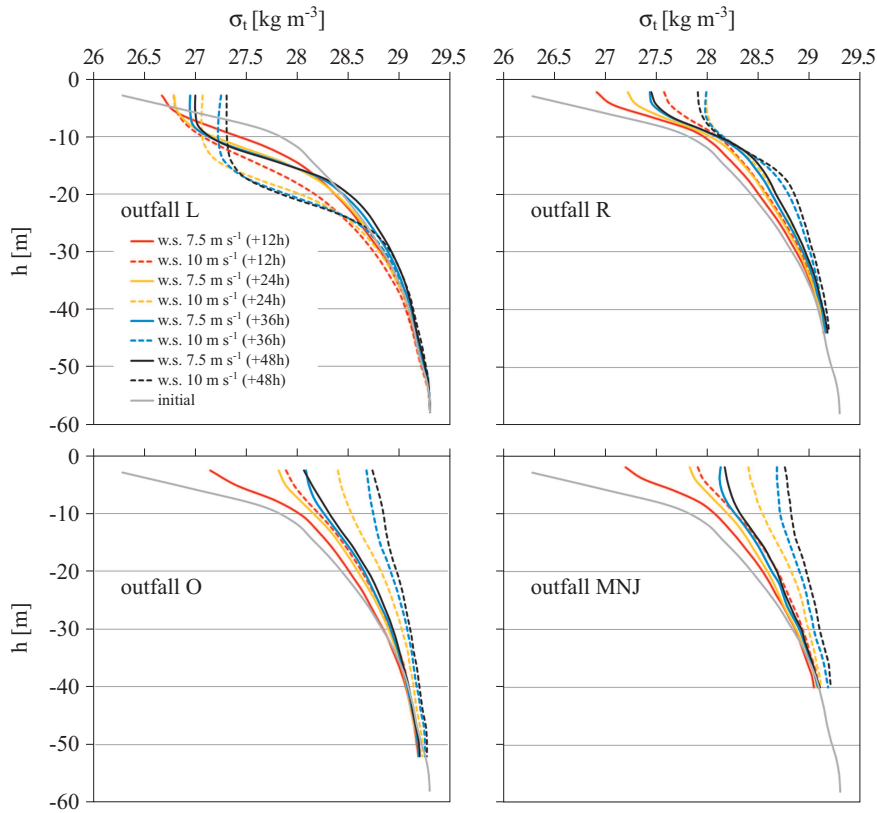
Figure 9. Vertical density profiles used in the near-field calculations at the locations L, R, O, MNJ planned for submarine outfall diffusers for a 48 h simulation time and a time step of 12 h (June/July)

of 48 h with a time step of 12 h (June/July). It can be seen that the most intense erosion of stratification appears during the first 12 h, because of intense surface cooling and pronounced vertical velocity shear between the surface outflow currents and the compensating bottom inflow, which enhance mixing.

The maximum rise height (minimum depth) of the effluent plume in the near-field simulations during 48 h and constant wind forcing with speeds of 7.5 m s^{-1} and 10 m s^{-1} (June/July) are shown in Figure 10. A wind speed increase from 7.5 m s^{-1} to 10 m s^{-1} has no significant impact on the maximum rise height at position L, since the vertical density structure in the bottom layer keeps the same gradient as before. Pronounced changes in the rise height of almost 10 m due to the wind speed increase (from 7.5 m s^{-1} to 10 m s^{-1}) are registered at positions O and MNJ. After 48 h of continuous wind forcing with a speed of 10 m s^{-1}, the density profiles tend
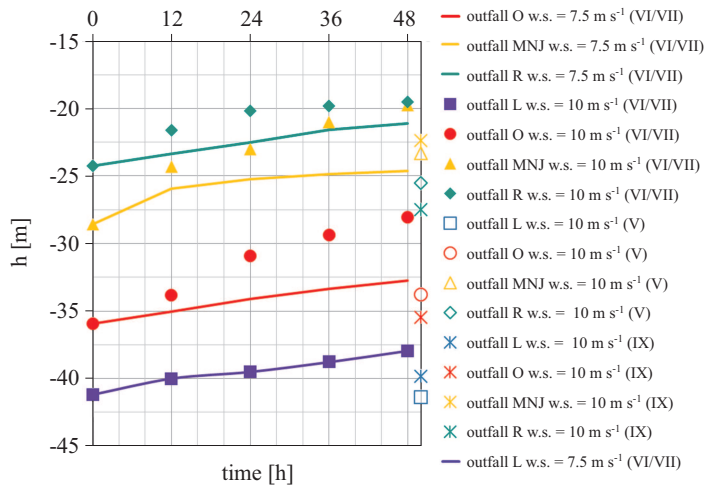
Figure 10. Near-field model results for effluent plume maximum rise heights (minimal depths) obtained from the experiments with 48 h of continuous 7.5 m s^{-1} and 10 m s^{-1} steady wind forcing and different density stratification (May/June/July/September)

to become well mixed. On the other hand, the increase in wind speed causes the formation of a prominent pycnocline layer in the depth range from 10 to 20 m at position R. Therefore, in the numerical experiment with a wind of 10 m s^{-1}, plume rise occurred only during the first 24 h of simulation whereas in the next 24 h the plume was captured back at 20 m depth. In the case of wind forcing with a 7.5 m s^{-1} plume, the depth at site R decreased during the whole experiment and after 48 h approached the 20 m level characteristic of a wind speed of 10 m s^{-1}. Figure 10 also indicates the maximum rise heights in May and September for 48 h continuous wind forcing with a wind speed of 10 m s^{-1}. Compared to the rise heights obtained in June/July, the effluent plume would be retained at even greater depths. The main cause lies in the stronger density gradients through the intermediate and bottom layer found during May and September.

Based on our model results, one can conclude that the analysed water body is safe in terms of effluent plume retention below the sea surface during the height of the tourist season, beginning in May and ending in September. Effluent plume rise to the sea surface can be expected only during the period of homogeneous vertical density distribution, which takes place in late October or November and lasts until the end of the April (Artegiani et al. 1997). It should be stressed that the analysis was performed for the synoptic condition that would most likely lead to vertical mixing of the water column during the summer: namely, the bora wind, owing to its high

speed and gustiness with cold air over the sea is the prime cause of vigorous mixing throughout the water column in the whole northern Adriatic, not only in the studied area of Rijeka Bay.

5. Conclusions

A three-dimensional numerical model, forced with the atmospheric wind and 7 major tidal constituents, was used to model the sea density changes in the vertical at the vicinity of submarine outfall diffuser sections. The four municipal submarine outfalls analysed are located within the model domain, covering the area of Rijeka Bay in Croatia. The relevant details of effluent plume rise reaching neutral buoyancy stagnation depths are resolved with the use of another numerical model, which takes only near-field process dynamics into consideration. The study focuses on the summer period, when stable density stratification should retain the effluent plumes below the surface layer. However, the stable summer stratification may be destroyed, primarily because of the cold, dry, strong bora wind, blowing across Rijeka Bay from the NE with an approximately steady speed and direction over a longer period. This kind of atmospheric disturbance disrupts the initial vertical density gradients and could be a cause of increased effluent plume rise towards the sea surface.

Stationary wind forcing characterized by a duration of 48 hours with wind speeds of 7.5 and 10 m s^{-1} was used during the 3D model simulations. Corresponding return periods for each individual situation analysed are assessed from the continuous 28-year data set obtained from the reference anemometer station at Rijeka. The results of numerical simulations, together with statistical analysis of the wind data, showed that the probability of density mixing in the vertical accompanied by effluent plume rise to the sea surface is extremely low in the period from May to September. The three-dimensional numerical model was verified with sea temperature vertical profiles measured at several stations located within the model domain. The differences between the measured and modelled sea temperatures in the intermediate and bottom layers are most probably due to the presence of bottom freshwater springs with typical inflow temperatures 10°C lower than in the rest of column.

The modelled current fields with stationary wind forcing showed that an increase in wind speed changes not only the vertical structure but also the horizontal current system owing to a deepening of the Ekman layer. The most intense erosion of the initial sea density profile can be expected within the first 12 h due to intense surface cooling and strong vertical velocity gradients between the outgoing surface and incoming compensatory bottom current.

Effluent plume rise during the first 48 h with constant wind forcing characterized by speeds of 7.5 and 10 m s^{-1} is almost the same at the position of submarine outfall L, but significantly different at sites O and MNJ. A continuous wind of 10 m s^{-1} speed and of 48 hours' duration will cause the density profiles at sites O and MNJ to mix. A higher wind speed at site R reduces the pycnocline layer thickness, inducing effluent plume rise during only the first 24 h of the simulation period. Furthermore, the simulation with a wind of 10 m s^{-1} speed and of 48 hours' duration resulted in a bigger effluent plume depth than in June/July owing to the stronger density gradients in the intermediate and bottom layers in May and September.

The results show that sea water quality, in terms of effluent plume retention below the sea surface, is independent of the bora wind's influence throughout the summer. Future studies should investigate the advection of the effluent plume in the far-field zone and the possibility of upwelling. Other synoptic situations having possible effects on summer vertical stratification should also be studied in more detail (e.g. sirocco wind events). Some new studies are already being carried out along these lines.

References

Akar P. J., Jirka G. H., 1994a, *Buoyant spreading processes in pollutant transport and mixing. Part 1: Lateral spreading with ambient current advection*, J. Hydraul. Res., 32 (6), 427–439.

Akar P. J., Jirka G. H., 1994b, *Buoyant spreading processes in pollutant transport and mixing. Part 2: Upstream spreading in weak ambient current*, J. Hydraul. Res., 33 (1), 24–37.

Andročec V., Beg-Paklar G., Dadić V., Djakovac T., Grbec B., Janeković I., Krstulovi N., Kušpilić G., Leder N., Lončar G., Marasović I., Precali R., Šolić M., 2009, *The Adriatic Sea Monitoring Program – final report*, MCEPP, Zagreb, Croatia.

Artegiani A., Bregant D., Paschini E., Pinardi N., Raicich F., Russo A., 1997, *The Adriatic Sea general circulation. Part I: Air-sea interactions and water mass structure*, J. Phys. Oceanogr., 27 (8), 1492–1514.

Beg Paklar G., 2000, *Influence of the bora wind on the northern Adriatic – simulations with the meteorological and oceanographic models*, Ph.D. thesis, Fac. Sci., Univ. Zagreb, 210 pp.

Bleninger T., 2007, *Coupled 3D hydrodynamic models for submarine outfalls: Environmental hydraulic design and control of multiport diffusers*, Diss. Inst. Hydromech., Univ. Karlsruhe, Heft 2006/3, 219 pp.

Cushman-Roisin B., Gualtieri C., Mihailović D. T., 2008, *Environmental fluid mechanics: Current issues and future outlook*, [in:] *Fluid mechanics of*

environmental interfaces, C. Gualtieri & D. T. Mihailović (eds.), Taylor & Francis, London, 1–13.

Featherstone R. E., 1984, *Mathematical models of the discharge of wastewater into a marine environment*, [in:] *An introductory to water quality modelling*, A. James (ed.), 1st edn., Wiley, Chichester, 150–162.

Fischer H. B., List E. J., Koh R. C. Y., Imberger J., Brooks N. H., 1979, *Mixing in inland and coastal waters*, Acad. Press, New York, 483 pp.

Hydroexpert, 1993, *Analysis of sea currents and temperatures at the location of ADRIA LNG terminal at Omišalj*, Fac. Civil Eng., Univ. Zagreb, Croatia.

Janeković I., Bobanović J., Kuzmić M., 2003, *The Adriatic Sea M2 and K1 tides by 3D model and data assimilation*, Geophys. Res. Abstr., 9, 203–217.

Janeković I., Kuzmić M., 2005, *Numerical simulation of the Adriatic Sea principal tidal constituents*, Ann. Geophys., 23 (10), 3207–3218.

Lončar G., 2010, *Comparing the models of effluent spreading in the near field zone resulting from operational coastal public sewerage system submarine outfalls*, Croat. Waters, 17 (69/70), 229–240.

Penzar B., Makjanić B., 1978, *Uvod u opću klimatologiju*, PMF – Sveučilište u Zagrebu, Zagreb, 205 pp.

Penzar B., Penzar I., Orlić M., 2001, *Vrijeme i klima hrvatskog Jadrana*, Nakladna kuća Dr. Feletar, Zagreb, 258 pp.

Pun K. L., Davidson M. J., 1999, *On the behaviour of advected plumes and thermals*, J. Hydraul. Res., 37 (4), 296–311.

Rodi W., 1987, *Examples of calculation methods for flow and mixing in stratified fluids*, J. Geophys. Res., 92 (C5), 5305–5328.

Roe P. L., 1981, *Approximate Riemann solvers, parameters vectors and difference schemes*, J. Comput. Phys., 43 (2), 357–372.

Sleigh D. H., Gaskel P. H., 1998, *An unstructured finite volume algorithm for predicting flow in rivers and estuaries*, Comput. Fluids, 27 (4), 479–508.

Smagorinsky J., 1993, *Some historical remarks on the use of nonlinear viscosities*, [in:] *Large eddy simulations of complex engineering and geophysical flows*, B. Galperin & S. Orszag (eds.), Cambridge Univ. Press, Cambrige, 1–34.

Song Y., Haidvogel D., 1994, *A semi-implicit ocean circulation model using a generalised topography-following coordinate system*, J. Comput. Phys., 115 (1), 228–244.

Supić N., Vilibić I., 2006, *Dense water characteristics in the northern Adriatic in the 1967–2000 interval with respect to surface fluxes and Po river discharge rates*, Estuar. Coast. Shelf Sci., 66 (3–4), 580–593.